PHYSICAL REVIEW B **110**, 184501 (2024)

Editors' Suggestion

Field-induced superconductivity mediated by odd-parity multipole fluctuation

Kosuke Nogaki[1,2,*] and Youichi Yanase[1]

[1]*Department of Physics, Kyoto University, Kyoto 606-8502, Japan*

[2]*RIKEN Center for Emergent Matter Science (CEMS), Wako 351-0198, Japan*

(Received 12 December 2023; revised 10 October 2024; accepted 11 October 2024; published 1 November 2024)

Field-induced superconductivity has long presented a counterintuitive phenomenon and a pivotal challenge in condensed matter physics. In this paper, we introduce a mechanism for achieving field-induced superconductivity wherein the sublattice degree of freedom and the Coulomb interaction are tightly entwined. Our multipole-resolved analysis elucidates that lifting the fluctuation degeneracy results in an unconventional Cooper pairing channel, thereby realizing field-induced superconductivity. This research substantively augments the exploration of the latent potential of strongly correlated electron systems with sublattice degrees of freedom.

DOI: 10.1103/PhysRevB.110.184501

I. INTRODUCTION

Superconductivity, which is typically suppressed by a magnetic field through both the Pauli and orbital-depairing effects [1], is paradoxically induced by the magnetic field in some systems. This counterintuitive phenomenon has garnered significant attention due to its implications for the unconventional origins of superconductivity. One of the well-known mechanisms of field-induced superconductivity is the Jaccarino-Peter effect [2,3], which states that the external magnetic field compensates for the internal field produced by magnetic ions. Notably, the Chevrel phase superconductor $Eu_xSn_{1-x}Mo_6S_8$ [4,5] and the organic superconductors λ-$(BETS)_2FeCl_4$ [6,7] and κ-$(BETS)_2FeBr_4$ [8] have been associated with the Jaccarino-Peter effect. In addition, the decrease of Kondo scattering [9,10] and the reduction of the quasiparticle renormalization effect [11] have also been discussed as other possible mechanisms.

Field-induced superconductivity in uranium-based superconductors, as observed in UGe_2 [12,13], URhGe [14,15], UCoGe [16,17], and UTe_2 [18–21], has been established experimentally. This class of phenomena has predominantly been attributed to changes in effective interactions for Cooper pairing, specifically the amplification of ferromagnetic fluctuations. The application of a magnetic field brings these systems closer to a quantum critical point, which in turn enhances the strength of effective interactions responsible for the observed field-induced superconductivity [22–30].

Recently, the discovery of field-induced parity transition in $CeRh_2As_2$ has illuminated the role of sublattice degrees of freedom in heavy-fermion systems [31]. Subsequent intensive experimental and theoretical works have demonstrated that local inversion symmetry breaking can enable Cooper pairs to form odd-parity pairings in the high-magnetic-field phase [32–58]. Interestingly, similar sublattice structures in the unit cells are also inherent in the uranium compounds mentioned earlier. In addition, field-induced superconductivity has been reported in a locally noncentrosymmetric cerium-based superconductor $CeSb_2$ [59,60] and in magic-angle twisted trilayer graphene [61,62]. Both uranium- and cerium-based superconductors, as well as moiré systems, may have superconducting states driven by electron correlation effects. Given this, theoretical studies focusing on the strong correlation effect, sublattice degrees of freedom, and the magnetic field are of significant interest. Indeed, the introduction of sublattice degrees of freedom leads to the emergence of *multipoles* within the systems, termed augmented multipoles, which are distributed throughout the unit cell [63–65]. The invoked interplay between superconductivity and multipole degrees of freedom has been the subject of extensive investigation [66–71]. However, most of the previous theoretical studies have been based on the weak-coupling theory. In particular, it should be noted that previous research has often assumed *degenerate* interactions in the sublattice degrees of freedom.

II. EFFECTIVE ACTION

In this paper, we introduce a mechanism for field-induced superconductivity that originates from *degeneracy-lifted* pairing interactions in sublattice degrees of freedom. A theoretical basis for strongly correlated superconductors is the following effective action:

$$\begin{aligned}\mathcal{S}_{\mathrm{eff}}[\bar{\psi},\psi] &= \mathcal{S}_{\mathrm{eff},0}[\bar{\psi},\psi] + \mathcal{S}_{\mathrm{eff,int}}[\bar{\psi},\psi]\\ &= \sum_{k}\bar{\psi}_{k,\alpha}(-i\omega_n\delta^{\alpha\beta} + \mathcal{H}_{\boldsymbol{k}}^{\alpha\beta} + \Sigma_k^{\alpha\beta})\psi_{k,\beta}\\ &\quad + \sum_{k,k',q}\bar{\psi}_{k+q,\alpha}\psi_{k,\beta}\Gamma_q^{\alpha\beta\gamma\delta}\bar{\psi}_{-k',\delta}\psi_{-k'+q,\gamma},\end{aligned} \tag{1}$$

where the abbreviated notations of $k = (\boldsymbol{k}, i\omega_n)$, $q = (\boldsymbol{q}, i\nu_n)$, and $\alpha = (s,\sigma)$ are employed. Here, the momentum $\boldsymbol{k}$ and the fermionic and bosonic Matsubara frequencies $\omega_n = (2n+1)\pi T$, $\nu_n = 2n\pi T$ stand for the space-time dependence of the electron field $\psi_{k,\alpha}$ and the correlation functions. The indexes s and σ represent the spin and sublattice degrees

*Contact author: kosuke.nogaki@riken.jp

of freedom, respectively. The $\mathcal{H}_{\boldsymbol{k}}^{\alpha\beta}$ is the single-particle Hamiltonian. We introduce the self-energy (Σ) and the vertex function (Γ); the former causes the renormalization of mass and damping of quasiparticles, while the latter drives the system toward superconductivity. These quantities obey the Ward-Takahashi identity: $\Sigma_k^{\alpha\beta} = \sum_q \Gamma_q^{\alpha\gamma\beta\delta} G_{k-q}^{\delta\gamma}$ [72,73]. Here, $G_k^{\alpha\beta} = -\langle \psi_{k,\alpha}\bar{\psi}_{k,\beta}\rangle$ describes the single-particle Green function. While the k and k' dependences of the vertex function are ignored for brevity, the extension of the following discussion to include such momentum dependence is straightforward [66,71].

By virtue of diagrammatic techniques (e.g., the fluctuation exchange (FLEX) approximation [74–76] or Parquet approximation [77,78]), the above effective action can be derived from a bare action,

$$\mathcal{S}_{\mathrm{bare}}[\bar{\psi},\psi] = \sum_k \bar{\psi}_{k,\alpha}(-i\omega_n\delta^{\alpha\beta} + \mathcal{H}_{\boldsymbol{k}}^{\alpha\beta})\psi_{k,\beta} + \sum_{k,k',q} \bar{\psi}_{k+q,\alpha}\psi_{k,\beta}\Gamma_q^{0,\alpha\beta\gamma\delta}\bar{\psi}_{-k',\delta}\psi_{-k'+q,\gamma}. \quad (2)$$

In this study, we focus on two-sublattice superconductors, including bilayer superconductors and twofold nonsymmorphic crystalline superconductors. In the bare action, $\mathcal{H}_{\boldsymbol{k}}^{\alpha\beta}$ represents the Hamiltonian of the two-sublattice system [44],

$$\mathcal{H}_{\boldsymbol{k}} = \varepsilon_{\boldsymbol{k}} s_0 \otimes \sigma_0 + \alpha \boldsymbol{g}_{\boldsymbol{k}} \cdot \boldsymbol{s} \otimes \sigma_z + t_\perp s_0 \otimes \sigma_x - \mu_{\mathrm{B}} H s_z \otimes \sigma_0. \quad (3)$$

Here, $\varepsilon_{\boldsymbol{k}} = -2t(\cos k_x + \cos k_y) + 4t'\cos k_x \cos k_y - \mu$ and $t_\perp$ represent intra- and intersublattice hopping term, respectively, and the sublattice-dependent $\boldsymbol{g}_{\boldsymbol{k}} \cdot \boldsymbol{s}$ term represents staggered Rashba-type spin-orbit coupling, which are originated from local inversion symmetry breaking [32,79–90]. The g-vector $\boldsymbol{g}_{\boldsymbol{k}} = [-\partial\varepsilon_{\boldsymbol{k}}/\partial k_y, \partial\varepsilon_{\boldsymbol{k}}/\partial k_x, 0]$ introduces the momentum- and sublattice-dependent spin polarization [91]. The H represents the Zeeman magnetic field parallel to the z axis. The interaction term in the bare action is the Hubbard-type on-site Coulomb repulsion,

$$\mathcal{S}_{\mathrm{bare,\,int}} = U \sum_\sigma \bar{\psi}_{i,\uparrow,\sigma}\psi_{i,\uparrow,\sigma}\bar{\psi}_{i,\downarrow,\sigma}\psi_{i,\downarrow,\sigma}. \quad (4)$$

The bare interaction tensor Γ^0 is obtained from the above Hubbard interaction (see Appendix A).

The internal degrees of freedom of the two-sublattice model are classified by the augmented multipole operator $\hat{\mathcal{Q}}$ [63–65],

$$\hat{\mathcal{Q}}^{\mu\nu} = \sum_k \bar{\psi}_{k+q,\alpha}\mathcal{Q}_{\alpha\beta}^{\mu\nu}\psi_{k,\beta}, \quad (5)$$

where $\mathcal{Q}^{\mu\nu} = \bar{s}^\mu \otimes \bar{\sigma}^\nu$ satisfies the normalization condition $\mathrm{tr}[\mathcal{Q}\mathcal{Q}^\dagger] = 1$. Here, $\bar{s}^\mu = s^\mu/\sqrt{2}$ ($\bar{\sigma}^\mu = \sigma^\mu/\sqrt{2}$) are the normalized Pauli and unit matrices. The completeness of the Pauli matrices and the unit matrix leads to the following identity:

$$\sum_{\mathcal{Q}} \bar{\mathcal{Q}}_{ij}\bar{\mathcal{Q}}_{kl} = \delta_{il}\delta_{jk}, \quad (6)$$

where δ_{ij} is Kronecker's delta. This identity facilitates the analysis of multipole-resolved fluctuations [92]. The interaction term $\mathcal{S}_{\mathrm{eff,\,int}}$ in the effective action can be expressed as the sum of the bilinear interaction of the multipoles [93–97],

$$\mathcal{S}_{\mathrm{eff,\,int}}[\bar{\psi},\psi] \approx \sum_{\mathcal{Q},q} \hat{\mathcal{Q}}_q V_q^{\mathcal{Q}} \hat{\mathcal{Q}}_{-q}, \quad (7)$$

where $V_q^{\mathcal{Q}} = \mathcal{Q}_{\alpha\beta}\Gamma_q^{\beta\alpha\gamma\delta}\mathcal{Q}_{\gamma\delta}$ describes the coupling constants of interaction between the augmented multipoles. For simplicity of the physical picture, interactions between different multipoles are omitted here, but they are appropriately taken into account later in the numerical calculations.

From the multipole-resolved interaction, a zero-momentum ($q = k - k' = 0$) Cooper pairing interaction can be obtained [66,71]. The intrasublattice even- and odd-parity multipole fluctuations, denoted by $\bar{\sigma}^0$ and $\bar{\sigma}^z$, result in the following Cooper pairing interactions [71]:

$$\mathcal{S}_{\sigma_0}[\bar{\psi},\psi] = \frac{1}{2}\sum_{k,k'} V_{k-k'}^{\sigma^0}\{\hat{\mathcal{P}}_k^{0,\dagger}\hat{\mathcal{P}}_{k'}^0 + \hat{\mathcal{P}}_k^{z,\dagger}\hat{\mathcal{P}}_{k'}^z + \hat{\mathcal{P}}_k^{x,\dagger}\hat{\mathcal{P}}_{k'}^x + \hat{\mathcal{P}}_k^{y,\dagger}\hat{\mathcal{P}}_{k'}^y\}, \quad (8)$$

$$\mathcal{S}_{\sigma_z}[\bar{\psi},\psi] = \frac{1}{2}\sum_{k,k'} V_{k-k'}^{\sigma^z}\{\hat{\mathcal{P}}_k^{0,\dagger}\hat{\mathcal{P}}_{k'}^0 + \hat{\mathcal{P}}_k^{z,\dagger}\hat{\mathcal{P}}_{k'}^z - \hat{\mathcal{P}}_k^{x,\dagger}\hat{\mathcal{P}}_{k'}^x - \hat{\mathcal{P}}_k^{y,\dagger}\hat{\mathcal{P}}_{k'}^y\}, \quad (9)$$

where $\hat{\mathcal{P}}^\mu = \psi_\alpha \bar{\sigma}_{\alpha\beta}^\mu \psi_\beta$ (see Appendix B). In the degenerate case, where even- and odd-parity multipole interactions have the same coupling constant (i.e., $V_{k-k'} := V_{k-k'}^{\sigma^0} = V_{k-k'}^{\sigma^z}$), we obtain

$$\mathcal{S}_{\mathrm{degenerate}} = \sum_{k,k'} V_{k-k'}\{\hat{\mathcal{P}}_k^{0,\dagger}\hat{\mathcal{P}}_{k'}^0 + \hat{\mathcal{P}}_k^{z,\dagger}\hat{\mathcal{P}}_{k'}^z\}. \quad (10)$$

This is simply the frequently assumed pairing interaction for two-sublattice models [32,80–85,88,98,99]. When the degeneracy is lifted, the second-line terms in Eqs. (8) and (9) could result in an unconventional intersublattice Cooper pairing channel. Field-induced superconductivity, a main result of this paper, is attributed to such degeneracy-lifted interactions, which are ubiquitous in strongly correlated systems.

The FLEX approximation extended to spin-orbit-coupled two-sublattice systems is employed to derive the effective action in this work [100–103] (see Appendix A). Hereafter, we set $t' = 0.3$, $\mu_{\mathrm{B}} = 1$, and $U = 3.9$ with a unit of energy $t = 1$ and determine the chemical potential so that the electron density per site is $n = 0.85$. In the numerical study, we use 64×64 $\boldsymbol{k}$ meshes, and 16 384, 8192, or 4096 Matsubara frequencies for $T = 0.004$, $0.004 < T < 0.01$, or $0.01 \leqslant T$, respectively.

III. ODD-PARITY MULTIPOLE FLUCTUATION

A. Phenomenology

In the FLEX approximation, the enhanced multipole susceptibilities are given by the following equation:

$$\chi_{\xi_1\xi_2\xi_3\xi_4}(q) = \chi_{\xi_1\xi_2\xi_3\xi_4}^{(0)}(q) + \chi_{\xi_1\xi_2\xi_5\xi_6}^{(0)}(q)U_{\xi_5\xi_6\xi_7\xi_8}\chi_{\xi_7\xi_8\xi_3\xi_4}(q), \quad (11)$$

where $\chi(q)$ and $\chi^{(0)}(q)$ are full and irreducible susceptibility tensors, respectively. Here, the abbreviated notation

$\xi = (s, \sigma)$ is adopted. Upon inserting Eq. (6), Eq. (11) can be reformulated into a multipole-resolved form as

$$\begin{aligned}\chi^{\mathcal{Q}}(q) &= \bar{\mathcal{Q}}_{\xi_1\xi_2}\chi_{\xi_2\xi_1\xi_3\xi_4}(q)\bar{\mathcal{Q}}_{\xi_3\xi_4} \\ &= \chi^{0,\mathcal{Q}}(q) + \sum_{\mathcal{Q}'}\chi^{0,\mathcal{Q}\mathcal{Q}'}U^{\mathcal{Q}'}\chi^{\mathcal{Q}'\mathcal{Q}} \\ &\approx \chi^{0,\mathcal{Q}}(q) + \chi^{0,\mathcal{Q}}(q)U^{\mathcal{Q}}\chi^{\mathcal{Q}}(q),\end{aligned} \tag{12}$$

where $U^{\mathcal{Q}} = \bar{\mathcal{Q}}_{\xi_1\xi_2}U_{\xi_1\xi_2\xi_3\xi_4}\bar{\mathcal{Q}}_{\xi_4\xi_3}$. In the final expression, the cross terms between different multipole terms, denoted as $\chi^{\mathcal{Q}\mathcal{Q}'} = \bar{\mathcal{Q}}_{\xi_1\xi_2}\chi_{\xi_1\xi_2\xi_3\xi_4}\bar{\mathcal{Q}}'_{\xi_4\xi_3}$, are ignored. Note that the cross term of interaction $U^{\mathcal{Q}\mathcal{Q}'}$ is absent due to the high symmetry of Eq. (4). Solving Eq. (12), we obtain the enhanced multipole susceptibility due to interactions,

$$\chi^{\mathcal{Q}}(q) \approx \frac{\chi^{0,\mathcal{Q}}(q)}{1 - U^{\mathcal{Q}}\chi^{0,\mathcal{Q}}(q)}. \tag{13}$$

A sufficient condition for achieving a large $\chi^{\mathcal{Q}}(q)$ entails having a large $\chi^{0,\mathcal{Q}}(q)$ and a positive U^{Q}. To reveal the criterion for realizing a large $\chi^{0,\mathcal{Q}}(q)$, here we discuss the multipole susceptibilities approximately derived without the self-energy,

$$\chi^{0,\mathcal{Q}}(q) = \sum_{\boldsymbol{k}} \mathcal{Q}^{\boldsymbol{k}-\boldsymbol{q},\boldsymbol{k}}_{\eta\zeta}\mathcal{Q}^{\boldsymbol{k},\boldsymbol{k}-\boldsymbol{q}}_{\zeta\eta}L_{\zeta\eta}(\boldsymbol{k},\boldsymbol{q},i\nu_n), \tag{14}$$

where $\mathcal{Q}^{\boldsymbol{k},\boldsymbol{k}'}_{\zeta\eta} = \langle u_{\zeta,\boldsymbol{k}}|\mathcal{Q}|u_{\eta,\boldsymbol{k}'}\rangle$ represents the matrix element of the multipole operator $\mathcal{Q}$, and $L_{\zeta\eta}(\boldsymbol{k},\boldsymbol{q},i\nu_n) = -\frac{1}{N}\{f(\varepsilon_{\eta,\boldsymbol{k}-\boldsymbol{q}}) - f(\varepsilon_{\zeta,\boldsymbol{k}})\}/\{i\nu_n + \varepsilon_{\eta,\boldsymbol{k}-\boldsymbol{q}} - \varepsilon_{\zeta,\boldsymbol{k}}\}$ is the momentum-resolved Lindhard function (see Appendix C). The eigenvector and eigenvalue of a band ζ of the Hamiltonian are denoted by $|u_{\zeta,\boldsymbol{k}}\rangle$ and $\varepsilon_{\zeta,\boldsymbol{k}}$. To activate the multipole $\mathcal{Q}$ fluctuation, a sizable matrix element $\mathcal{Q}^{\boldsymbol{k}-\boldsymbol{q},\boldsymbol{k}}_{\eta\zeta}$ and a positive interaction for the multipole, $U^{\mathcal{Q}} > 0$, are required. Thus, the electronic structure of the system inherently dictates the enhanced multipole fluctuation. Note that the approximated expressions (12)–(14) are used only to grasp the physical idea and to interpret the numerical results. The numerical calculations are carried out with the full FLEX approximations and the above approximations are not adopted.

B. Electronic band structure and wave function

Herein, we demonstrate that a two-sublattice structure intrinsically favors odd-parity multipole fluctuations. Figure 1(a) illustrates the Fermi surfaces (FSs) of our two-sublattice tight-binding model with two bands, labeled $|1\rangle$ and $|2\rangle$. Our system exhibits a type-II van Hove singularity (vHS) resulting from the Rashba-type spin-orbit coupling [104–106]. Specifically, the type-II vHS is located around $\boldsymbol{k} = (\pm\delta, \pi)$, $(0, \pi \pm \delta)$, $(\pi, \pm\delta)$, and $(\pi \pm \delta, 0)$. Figure 1(a) displays the expectation values of the inversion symmetry operator, $\mathcal{I} = s_0 \otimes \sigma_x$, on the FSs. The bonding and antibonding orbitals, defined as

$$|\mathrm{BO}\rangle \equiv \frac{1}{\sqrt{2}}\begin{pmatrix}1\\1\end{pmatrix}_{\sigma}, \tag{15}$$

$$|\mathrm{ABO}\rangle \equiv \frac{1}{\sqrt{2}}\begin{pmatrix}1\\-1\end{pmatrix}_{\sigma}, \tag{16}$$

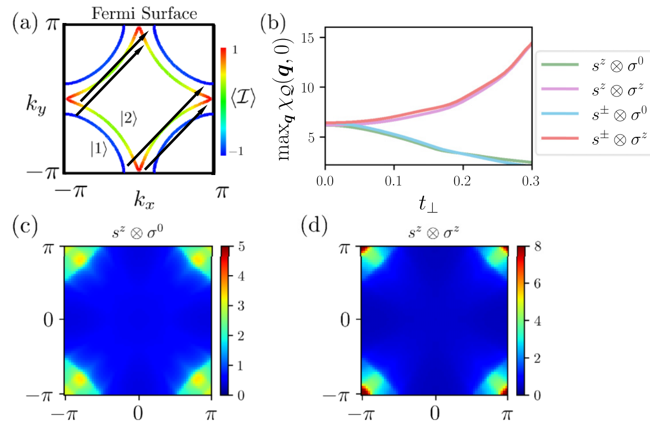

FIG. 1. (a) The Fermi surface of the two-sublattice tight-binding model with the model parameters $\alpha = 0.2$, $t_\perp = 0.2$. The coloration on the Fermi surface signifies the expectation value of the inversion symmetry operator $\mathcal{I} = s_0 \otimes \sigma_x$. (b) The intersublattice hopping $t_\perp$ dependence of static multipole fluctuations obtained by the FLEX approximations. The maximum of the even-parity (odd-parity) longitudinal (transverse) magnetic multipole susceptibilities is shown. Other multipole fluctuations are negligibly small. We assume $\alpha = 0.2$, $t_\perp = 0.2$, and $T = 0.01$. (c),(d) The momentum dependence of the even-parity and odd-parity longitudinal magnetic susceptibilities, respectively.

satisfy $\mathcal{I}|\mathrm{BO}\rangle = |\mathrm{BO}\rangle$ and $\mathcal{I}|\mathrm{ABO}\rangle = -|\mathrm{ABO}\rangle$. Considering that the expectation values of $\mathcal{I}$ on the FSs are close to ± 1, we find that the wave functions around the type-II vHS are well approximated by either the bonding or antibonding orbitals.

In itinerant electron systems, multipole fluctuations emerge from the nesting of FSs especially around vHS [107,108]. Two potential nesting scenarios exist: one involves nesting within the same FSs, either bonding to bonding or antibonding to antibonding. The other involves nesting between different FSs, i.e., bonding to antibonding. The nesting vectors corresponding to each of these scenarios are illustrated in Fig. 1(a). Employing the previously approximated wave functions, we can roughly evaluate the matrix element of the sublattice operator: $\langle 1|\sigma^0|1\rangle \approx \langle 1|\sigma^z|2\rangle \approx 1$ and $\langle 1|\sigma^0|2\rangle \approx \langle 1|\sigma^z|1\rangle \approx 0$. Notably, while the nesting vectors connecting the same FSs are not equivalent to each other, those connecting different FSs are equivalent. Furthermore, the Hubbard-type Coulomb interaction can be expressed in the multipole basis as

$$\mathcal{S}_{\mathrm{int}} = -\frac{U}{4}\sum_{\nu=0,z}\hat{\mathcal{Q}}^{0\nu}_{q}\hat{\mathcal{Q}}^{0\nu}_{-q} + \frac{U}{4}\sum_{\substack{\mu=x,y,z\\ \nu=0,z}}\hat{\mathcal{Q}}^{\mu\nu}_{q}\hat{\mathcal{Q}}^{\mu\nu}_{-q}. \tag{17}$$

This expression for the multipole-resolved interaction implies that the Coulomb interaction equally enhances the even-parity and odd-parity magnetic multipoles. As a result, in the two-sublattice model, odd-parity multipole fluctuations are expected to be strongly enhanced by nesting of different FSs and Coulomb interaction, especially for large $t_\perp$ and chemical potentials near the vHS.

C. Numerical results

While the above phenomenological arguments are not assumed in our numerical calculations, where spin and sublattice degrees of freedom are exactly dealt with, the above expectation is verified by the numerical results. Figure 1(b) depicts the dependence of multipole fluctuations on $t_\perp$, microscopically calculated using the FLEX approximation. As the intersublattice hopping parameter $t_\perp$ increases, odd-parity fluctuations are notably enhanced while even-parity fluctuations are suppressed, consistent with the above discussions. Figures 1(c) and 1(d) show the momentum dependence of multipole susceptibilities. The even-parity longitudinal magnetic fluctuation represented by the multipole operator $\mathcal{Q}^{z0} = \bar{s}^z \otimes \bar{\sigma}^0$ exhibits a double-peak structure around $\boldsymbol{Q} \sim (\pi, \pi)$ and $(\pi - \delta, \pi - \delta)$ [Fig. 1(c)]. In contrast, the odd-parity longitudinal magnetic fluctuation given by the multipole operator $\mathcal{Q}^{zz} = \bar{s}^z \otimes \bar{\sigma}^z$ presents a single-peak structure around $\boldsymbol{Q} \sim (\pi, \pi)$ [Fig. 1(d)]. These findings further substantiate the previous analysis of the nesting and wave functions of the FSs, offering a more quantitative view. Note that the transverse magnetic fluctuations manifest a similar momentum dependence to the longitudinal ones. This is a consequence of the momentum dependence of Rashba spin-orbit coupling which tends to vanish around vHS.

IV. SUPERCONDUCTIVITY

Here we study superconductivity predominantly mediated by the odd-parity multipole fluctuations using the linearized Éliashberg equation (see Appendix E). Figure 2(a) depicts the magnetic field dependence of the eigenvalues of this equation. In the left figure for $t_\perp = 0.1$, the typical behavior of superconductivity under an external magnetic field is evident. All eigenvalues across all irreducible representations are suppressed by the magnetic field. Notably, at $H = 0.22$, the eigenvalue curves of the B_g and B_u representations intersect. This intersection signals a phase transition from even-parity to odd-parity superconductivity, reminiscent of phenomena observed in $CeRh_2As_2$ [31,44,82]. Evident from Fig. 1(b), multipole susceptibilities nearly degenerate at $t_\perp = 0.1$ and, therefore, the effective interaction has nearly isotropic form in the sublattice space. Thus, the mechanism of the parity transition in the left figure of Fig. 2(a) is essentially the same as that discussed in $CeRh_2As_2$ [31,44,82]. In contrast, at $t_\perp = 0.2$ [right figure of Fig. 2(a)], the eigenvalue for the B_u representation increases upon magnetic field application, while that of B_g diminishes. Such behavior suggests the possible emergence of field-induced odd-parity superconductivity in the two-sublattice strongly correlated electron systems.

We delve into the mechanism behind this field-induced superconductivity. Initially, the intrasublattice pair potential, given by $\Delta^{\text{intra}}_{B_u}(k) = \psi(\boldsymbol{k}) i s_y \otimes \sigma_z + \boldsymbol{d}(\boldsymbol{k}) \cdot \boldsymbol{s}\, i s_y \otimes \sigma_0$, is illustrated in Figs. 2(b)–2(d). Influenced by the antiferromagnetic fluctuation, the spin-singlet component shows a $d_{x^2-y^2}$-wave form. In addition, the spin-triplet components induced by the spin-orbit coupling display a p-wave momentum dependence. Interestingly, these gap functions are relatively impervious to the external magnetic field [31,44,82]. Subsequently, the intersublattice pair potentials are analyzed. In Fig. 2(e), the component-resolved magnetic field dependence of intersublattice gap functions is shown. Evidently, the magnetic field induces a sizable spin-triplet and sublattice-antisymmetric pair potential,

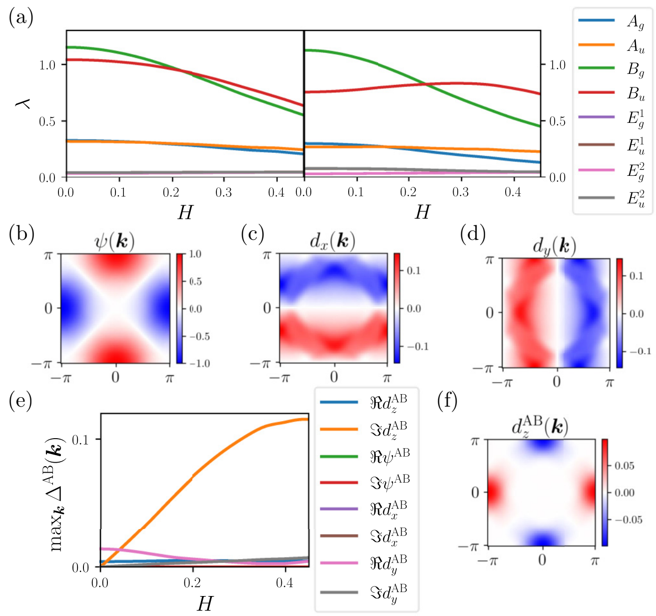

FIG. 2. (a) The magnetic field dependence of eigenvalues of the Éliashberg equation for each irreducible representation. We assume $\alpha = 0.2$ and $T = 0.01$. Left: $t_\perp = 0.1$. Right: $t_\perp = 0.2$. Superconducting instabilities are classified by the irreducible representation of the point group of the system, C_{4h}. The superscript of $E^{1,2}_{g/u}$ representations expresses the degeneracy lifted by time-reversal symmetry breaking due to the magnetic field. As the temperature decreases, the eigenvalues of the Éliashberg equation increase and eventually exceed unity at a sufficiently low temperature. (b)–(d) The momentum dependence of intrasublattice spin-singlet and spin-triplet gap functions, $\psi(\boldsymbol{k})$ and $\boldsymbol{d}(\boldsymbol{k})$, of the B_u representation for $H = 0.15$. Results for the B_g representation are almost the same as the figures. (e) The magnetic field dependence of the component-resolved weight of the intersublattice gap function. (f) The momentum dependence of the intersublattice spin-triplet gap function, $\mathrm{Im} d_z^{\mathrm{AB}}(\boldsymbol{k})$.

$$\mathrm{Im} d_z^{\mathrm{AB}}(\boldsymbol{k}) s_z i s_y \otimes \sigma_y, \tag{18}$$

which is prohibited at the zero magnetic field by time-reversal symmetry. The momentum dependence of this pair potential is depicted in Fig. 2(f). Notably, Eq. (18) represents a σ_y component in the sublattice degree of freedom. This implies that the pairing channel of $\mathcal{P}^y_k$ in Eqs. (8) and (9), which arises from the lifting of degeneracy between even-parity and odd-parity multipole fluctuations, plays a pivotal role in the manifestation of field-induced superconductivity. In essence, the Cooper pairing inherent in Eq. (18) is fundamentally rooted in the multipole-mediated interactions, given by Eqs. (8) and (9), and the disruption of the time-reversal symmetry by the external magnetic field allows this pairing to emerge. As a result, the field-induced superconductivity occurs in the two-sublattice system through a cooperative interplay

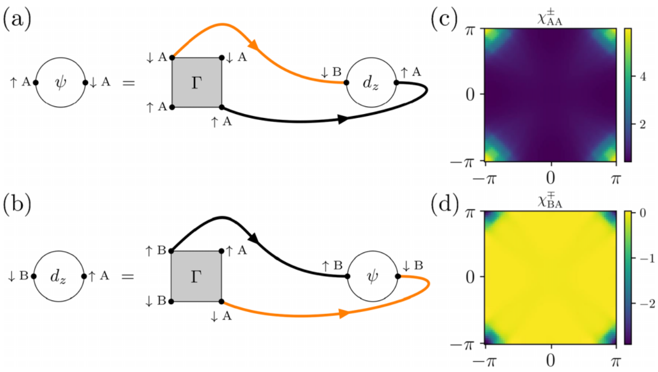

FIG. 3. (a),(b) The diagrammatic representation of the dominant scattering process between the Cooper pairs represented by $\psi^{\rm AA}$, $\psi^{\rm BB}$, and $d_z^{\rm AB}$. The black line and orange line represent the intrasublattice Green function $G^{\rm AA}(k)$ and the intersublattice Green function $G^{\rm AB}(k)$, respectively. The scattering process between $d_z^{\rm AB}$ and $\psi^{\rm AA}$ or $\psi^{\rm BB}$ via the transverse magnetic fluctuation are shown. (c) The momentum dependence of the intrasublattice transverse magnetic fluctuation which appears in diagram (a). (d) The momentum dependence of the intersublattice transverse magnetic fluctuation which appears in diagram (b).

between the odd-parity multipole fluctuation and the magnetic field.

Further support for our interpretation of the mechanism behind field-induced superconductivity comes from considerations based on Feynman diagram analyses for the Éliashberg equation. The gap function outlined in Eq. (18) plays a crucial role in facilitating the coupling between intrasublattice gap functions through a second-order scattering process. While simplification is attained by solely considering the transverse spin fluctuation denoted by $\chi^{\pm}$ or $\chi^{\mp}$, expanding the following analysis to include longitudinal spin fluctuation χ^{zz} is straightforward. In the following, we denote the dominant intrasublattice spin-singlet component in the A and B sublattices as $\psi^{\rm AA}(\boldsymbol{k})$ and $\psi^{\rm BB}(\boldsymbol{k})$, respectively.

The scattering processes illustrated in Figs. 3(a) and 3(b) highlight how the unusual intersublattice pairing, represented by ${\rm Im}d_z^{\rm AB}(\boldsymbol{k})s_z is_y \otimes \sigma_y$, introduces the attractive force between $\psi^{\rm AA}(\boldsymbol{k})$ and $\psi^{\rm BB}(\boldsymbol{k})$. By amalgamating these two diagrams and tracing out the gap function $d_z^{\rm BA}$, a composite diagram elucidating the second-order scattering process between $\psi^{\rm AA}(\boldsymbol{k})$ and $\psi^{\rm BB}(\boldsymbol{k})$ is derived. Due to the positive sign of $\chi^{\pm}_{\rm AA}$ and the negative sign of $\chi^{\mp}_{\rm BA}$ [see Figs. 3(c) and 3(d)], the overall sign of this second-order scattering process is negative. This scattering process with negative sign necessitates a sign change of gap functions through $2\boldsymbol{q} = (0, 0)$ momentum transfer, a condition intrinsically met due to the relation $\psi^{\rm AA}(\boldsymbol{k}) = -\psi^{\rm BB}(\boldsymbol{k})$. Notably, spin-orbit coupling is not required in this mechanism, thereby implying that field-induced superconductivity can be achieved in materials with weak spin-orbit coupling.

V. PHASE DIAGRAM

Figures 4(a)–4(d) show the phase diagrams for $\alpha/t_\perp = 0$, 0.5, 1, and 2 with $t_\perp = 0.2$. As expected, the odd-parity superconducting state exhibits field-induced behaviors in all cases. It is noteworthy that even in the case of $\alpha = 0$ (i.e., without spin-orbit coupling), the external magnetic field induces the odd-parity superconducting phase. Thus, the field-induced superconductivity does not require spin-orbit coupling. This phenomenon can be attributed to the strong-coupling effect that is anticipated in strongly correlated electron systems. A considerable interband gap function in combination to the field-induced pairing interaction could be responsible for the significant condensation energy, which in turn leads to the emergence of field-induced superconductivity. However, larger spin-orbit coupling renders the field-induced odd-parity superconducting phase more stable, as the transition temperature increases. Indeed, with spin-orbit coupling, the gap

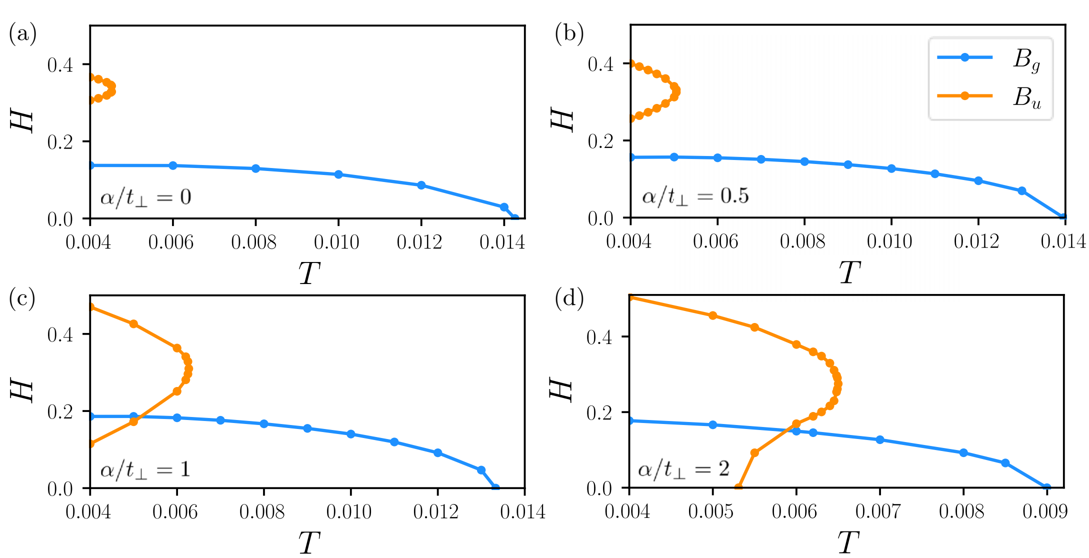

FIG. 4. (a)–(d) H-T phase diagrams of the two-sublattice Rashba-Hubbard model for $\alpha/t_\perp = 0$, 0.5, 1, 2. We show the superconducting transition lines of the even-parity B_g and odd-parity B_u states, on which eigenvalues of the Éliashberg equation become unity. The intersublattice hopping parameter $t_\perp$ is set to 0.2 for all cases.

function in Eq. (18) incorporates intraband components,

$$\Delta^{\pm}(\boldsymbol{k}) = \frac{d_z^{\mathrm{AB}}(\boldsymbol{k})}{|\boldsymbol{g}(\boldsymbol{k})|^2 + t_\perp^2}\{\mp\tilde{\boldsymbol{d}}\cdot\tilde{\boldsymbol{s}} + i\tilde{\psi}(\boldsymbol{k})\tilde{s}_0\}i\tilde{s}_y, \tag{19}$$

where $\tilde{\psi}(\boldsymbol{k}) = |\boldsymbol{g}(\boldsymbol{k})|^2$ and $\tilde{\boldsymbol{d}} = [g_y(\boldsymbol{k}), g_x(\boldsymbol{k}), 0]$. Consequently, the spin-orbit coupling significantly enhances the thermodynamic stability of the odd-parity superconducting phase.

The field-induced odd-parity superconducting state suffers from the Pauli depairing effect of Cooper pairs at extremely high fields, $H > 0.3$. Thus, the observed nonmonotonic behavior of the phase transition line of the B_u state can result from the competition between the field-enhancement mechanism, associated with the intersublattice gap function, and the Pauli depairing effect.

VI. SUMMARY

In summary, we have conducted a multipole-resolved analysis for unconventional superconductivity in strongly correlated two-sublattice systems. The lifting of degeneracy between even- and odd-parity multipole fluctuations gives rise to the unconventional pairing channel. We demonstrated that the two-sublattice structure inherently favors multipole fluctuations with a predominating odd-parity nature, which induce sublattice-antisymmetric pairing only when the magnetic field is applied. Consequently, the field-induced superconductivity occurs. Notably, the obtained phase diagram reveals the field-reentrant odd-parity superconducting states.

Field-induced superconductivity within the bilayer model has also been proposed in previous studies [109–113]. In these theories, a magnetic field is posited to shift the energy levels of electronic states, thereby facilitating unconventional interband Cooper pairing. However, these models assume isotropic interaction within the layers, which distinctly sets them apart from our mechanism. Note that the cornerstone of our proposal is the anisotropic effective interaction, a direct result of the degeneracy-lifted multipole fluctuations.

Finally, we would like to highlight a possible application of our theory. The electronic structure of magic-angle twisted trilayer graphene consists of a flat band from the moiré structure and a dispersive Dirac band in the absence of a displacement field [114–116]. The flat band potentially enhances the degenerated multipole fluctuation ensured by symmetry. For instance, 15-fold degenerate fluctuations protected by SU(4) symmetry have been proposed in magic-angle twisted bilayer graphene [117]. The introduction of a displacement field leads to the hybridization of these bands, which could result in the lifting of the degeneracy in multipole fluctuations [62]. Application of an external magnetic field possibly induces unconventional Cooper pairing, as discussed in this paper. This mechanism might explain the magnetic field-reentrant superconductivity observed in magic-angle twisted trilayer graphene [62]. Other potential candidates include uniaxially strained $CeRh_2As_2$ and pressurized $CeSb_2$ [60]. The pressure amplifies the intersublattice hopping and leads to the degeneracy-lifted multipole fluctuations. Comprehensive investigations into these phenomena are still highly anticipated.

ACKNOWLEDGMENTS

The authors are grateful to A. Daido, S. Sumita, and R. Oiwa for fruitful discussions. Some figures in this work were created by using FERMISURFER [118]. This work was supported by JSPS KAKENHI (Grants No. JP21K18145, No. JP22H04933, No. JP22H01181, No. JP22KJ1716, No. JP23K17353, No. JP24H00007, No. JP24K21530, and No. JP24K22869).

APPENDIX A: SELF-CONSISTENT CONDITION FOR FLUCTUATION EXCHANGE APPROXIMATION

The noninteracting Green functions for $U = 0$ are expressed by the 4×4 matrix form in the spin and sublattice basis,

$$G^{(0)}(\boldsymbol{k}, i\omega_n) = (i\omega_n s_0 \otimes \sigma_0 - \mathcal{H}_{\boldsymbol{k}})^{-1}, \tag{A1}$$

where $\omega_n = (2n+1)\pi T$ and $\mathcal{H}_{\boldsymbol{k}}$ are the fermionic Matsubara frequencies and Hamiltonian. Here, s and σ represent spin and sublattice degrees of freedom, respectively. In the interacting case $U \neq 0$, the dressed Green functions contain a self-energy $\Sigma(k)$,

$$G(k) = [i\omega_n s_0 \otimes \sigma_0 - \mathcal{H}_{\boldsymbol{k}} - \Sigma(k)]^{-1}. \tag{A2}$$

In the FLEX approximation, the self-energy is expressed with the use of an effective interaction $\Gamma^n(q)$ as

$$\Sigma_{\xi\xi'}(k) = \frac{T}{N}\sum_q \Gamma^n_{\xi\xi_1\xi'\xi_2}(q) G_{\xi_1\xi_2}(k-q), \tag{A3}$$

and the effective interaction is given by

$$\begin{aligned}\Gamma^n_{\xi_1\xi_2\xi_3\xi_4}(q) &= U_{\xi_1\xi_2\xi_5\xi_6}\chi_{\xi_5\xi_6\xi_7\xi_8}(q)U_{\xi_7\xi_8\xi_3\xi_4} \\ &\quad - \frac{1}{2}U_{\xi_1\xi_2\xi_5\xi_6}\chi^{(0)}_{\xi_5\xi_6\xi_7\xi_8}(q)U_{\xi_7\xi_8\xi_3\xi_4},\end{aligned} \tag{A4}$$

where $U_{\xi_1\xi_2\xi_3\xi_4}$ is the bare interaction tensor which satisfies the following relation:

$$\sum_{\xi_1\xi_2\xi_3\xi_4} U_{\xi_1\xi_2\xi_3\xi_4} c^\dagger_{\xi_1} c_{\xi_2} c_{\xi_3} c^\dagger_{\xi_4} = U\sum_{i,\sigma} n_{i\uparrow\sigma} n_{i\downarrow\sigma}, \tag{A5}$$

$$U_{\xi_1\xi_2\xi_3\xi_4} = \delta_{\sigma_1,\sigma_2}\delta_{\sigma_2,\sigma_3}\delta_{\sigma_3,\sigma_4} U_{s_1s_2s_3s_4}, \tag{A6}$$

$$U_{\uparrow\downarrow\uparrow\downarrow} = U_{\downarrow\uparrow\downarrow\uparrow} = -U_{\uparrow\uparrow\downarrow\downarrow} = -U_{\downarrow\downarrow\uparrow\uparrow} = U, \tag{A7}$$

and $i\nu_n$ are bosonic Matsubara frequencies. Here, $\chi(q)$ is the generalized susceptibility. The abbreviated notation $\xi = (s, \sigma)$ is employed. We introduce the bare susceptibility,

$$\chi^{(0)}_{\xi_1\xi_2\xi_3\xi_4}(q) = -\frac{T}{N}\sum_k G_{\xi_1\xi_3}(k) G_{\xi_4\xi_2}(k-q), \tag{A8}$$

and compute the generalized susceptibility by

$$\begin{aligned}\chi_{\xi_1\xi_2\xi_3\xi_4}(q) &= \chi^{(0)}_{\xi_1\xi_2\xi_3\xi_4}(q) \\ &\quad + \chi^{(0)}_{\xi_1\xi_2\xi_5\xi_6}(q) U_{\xi_5\xi_6\xi_7\xi_8}\chi_{\xi_7\xi_8\xi_3\xi_4}(q).\end{aligned} \tag{A9}$$

According to Eqs. (A2)–(A9), G, Σ, Γ^n, $\chi^{(0)}$, and χ depend on each other and, therefore, we self-consistently determine these functions. The FLEX approximation is a conserving approximation in which several conservation laws are satisfied in the framework of the Luttinger-Ward theory [100–103].

For functions with fermionic Matsubara frequencies $A(\boldsymbol{q}, i\omega_n)$, the static limit $A(\boldsymbol{q}, 0)$ is evaluated by an approximation justified at low temperatures,

$$A(\boldsymbol{q},0) \simeq \frac{A(\boldsymbol{q}, i\pi T) + A(\boldsymbol{q}, -i\pi T)}{2}. \tag{A10}$$

For the analysis of the superconducting phase transition, the particle-particle channel irreducible vertex function Γ^a is needed, and it is obtained by

$$\Gamma^a_{\xi_1\xi_2\xi_3\xi_4}(q) = U_{\xi_1\xi_2\xi_3\xi_4}/2 + U_{\xi_1\xi_2\xi_5\xi_6}\chi_{\xi_5\xi_6\xi_7\xi_8}(q)U_{\xi_7\xi_8\xi_3\xi_4}. \tag{A11}$$

APPENDIX B: COOPER PAIRING CHANNEL FROM MULTIPOLE FLUCTUATIONS

In this Appendix, we give a comprehensive classification of Cooper pairing channels mediated by multipole fluctuations. First, we summarize Cooper pairing channel decomposition in the presence of a single degree of freedom, σ,

$$\begin{aligned}\mathcal{S}^{\sigma_0} &= \bar{\psi}_\alpha\sigma^0_{\alpha\beta}\psi_\beta V^{\sigma^0}\bar{\psi}_\gamma\sigma^0_{\gamma\delta}\psi_\delta \\ &= \tfrac{1}{2}V^{\sigma^0}\{\hat{\mathcal{P}}^{0,\dagger}\hat{\mathcal{P}}^0 + \hat{\mathcal{P}}^{x,\dagger}\hat{\mathcal{P}}^x + \hat{\mathcal{P}}^{y,\dagger}\mathcal{P}^y + \hat{\mathcal{P}}^{z,\dagger}\mathcal{P}^z\},\end{aligned} \tag{B1}$$

$$\begin{aligned}\mathcal{S}^{\sigma_x} &= \bar{\psi}_\alpha\sigma^x_{\alpha\beta}\psi_\beta V^{\sigma^x}\bar{\psi}_\gamma\sigma^x_{\gamma\delta}\psi_\delta \\ &= \tfrac{1}{2}V^{\sigma^x}\{\hat{\mathcal{P}}^{0,\dagger}\hat{\mathcal{P}}^0 + \hat{\mathcal{P}}^{x,\dagger}\hat{\mathcal{P}}^x - \hat{\mathcal{P}}^{y,\dagger}\hat{\mathcal{P}}^y - \hat{\mathcal{P}}^{z,\dagger}\hat{\mathcal{P}}^z\},\end{aligned} \tag{B2}$$

$$\begin{aligned}\mathcal{S}^{\sigma_y} &= \bar{\psi}_\alpha\sigma^y_{\alpha\beta}\psi_\beta V^{\sigma^y}\bar{\psi}_\gamma\sigma^y_{\gamma\delta}\psi_\delta \\ &= \tfrac{1}{2}V^{\sigma^x}\{-\hat{\mathcal{P}}^{0,\dagger}\hat{\mathcal{P}}^0 + \hat{\mathcal{P}}^{x,\dagger}\hat{\mathcal{P}}^x - \hat{\mathcal{P}}^{y,\dagger}\hat{\mathcal{P}}^y + \hat{\mathcal{P}}^{z,\dagger}\hat{\mathcal{P}}^z\},\end{aligned} \tag{B3}$$

$$\begin{aligned}\mathcal{S}^{\sigma_z} &= \bar{\psi}_\alpha\sigma^z_{\alpha\beta}\psi_\beta V^{\sigma^z}\bar{\psi}_\gamma\sigma^z_{\gamma\delta}\psi_\delta \\ &= \tfrac{1}{2}V^{\sigma^x}\{\hat{\mathcal{P}}^{0,\dagger}\hat{\mathcal{P}}^0 - \hat{\mathcal{P}}^{x,\dagger}\hat{\mathcal{P}}^x - \hat{\mathcal{P}}^{y,\dagger}\hat{\mathcal{P}}^y + \hat{\mathcal{P}}^{z,\dagger}\hat{\mathcal{P}}^z\},\end{aligned} \tag{B4}$$

where the Cooper pair operators are defined by $\hat{\mathcal{P}}^\mu = \psi_\alpha\sigma^\mu_{\alpha\beta}\psi_\beta$. Here, the following identities on the Pauli and unit matrix are used [71]:

$$\sigma^0_{\alpha\beta}\sigma^0_{\gamma\delta} = \tfrac{1}{2}\left(\sigma^0_{\alpha\gamma}\sigma^0_{\delta\beta} + \sigma^x_{\alpha\gamma}\sigma^x_{\delta\beta} + \sigma^y_{\alpha\gamma}\sigma^y_{\delta\beta} + \sigma^z_{\alpha\gamma}\sigma^z_{\delta\beta}\right), \tag{B5}$$

$$\sigma^x_{\alpha\beta}\sigma^x_{\gamma\delta} = \tfrac{1}{2}\left(\sigma^0_{\alpha\gamma}\sigma^0_{\delta\beta} + \sigma^x_{\alpha\gamma}\sigma^x_{\delta\beta} - \sigma^y_{\alpha\gamma}\sigma^y_{\delta\beta} - \sigma^z_{\alpha\gamma}\sigma^z_{\delta\beta}\right), \tag{B6}$$

$$\sigma^y_{\alpha\beta}\sigma^y_{\gamma\delta} = \tfrac{1}{2}\left(-\sigma^0_{\alpha\gamma}\sigma^0_{\delta\beta} + \sigma^x_{\alpha\gamma}\sigma^x_{\delta\beta} - \sigma^y_{\alpha\gamma}\sigma^y_{\delta\beta} + \sigma^z_{\alpha\gamma}\sigma^z_{\delta\beta}\right), \tag{B7}$$

$$\sigma^z_{\alpha\beta}\sigma^z_{\gamma\delta} = \tfrac{1}{2}\left(\sigma^0_{\alpha\gamma}\sigma^0_{\delta\beta} - \sigma^x_{\alpha\gamma}\sigma^x_{\delta\beta} - \sigma^y_{\alpha\gamma}\sigma^y_{\delta\beta} + \sigma^z_{\alpha\gamma}\sigma^z_{\delta\beta}\right). \tag{B8}$$

Next, for the multipole composed of spin and sublattice degrees of freedom, as in the case of our model, we obtain the Cooper pairing channel as follows:

$$\begin{aligned}\mathcal{S}^{\mathcal{Q}} &= \bar{\psi}_\alpha\mathcal{Q}^{\mu\nu}_{\alpha\beta}\psi_\beta V^{\mathcal{Q}}\bar{\psi}_\gamma\mathcal{Q}^{\mu\nu}_{\gamma\delta}\psi_\delta \\ &= \bar{\psi}_{s_\alpha\sigma_\alpha}\bar{s}^\mu_{s_\alpha s_\beta}\bar{\sigma}^\nu_{\sigma_\alpha\sigma_\beta}\psi_{s_\beta\sigma_\beta}V^{\mathcal{Q}}\bar{\psi}_{s_\gamma\sigma_\gamma}\bar{s}^\mu_{s_\gamma s_\delta}\bar{\sigma}^\nu_{\sigma_\gamma\sigma_\delta}\psi_{s_\delta\sigma_\delta} \\ &= V^{\mathcal{Q}}\bar{\psi}_{s_\alpha\sigma_\alpha}\bar{\psi}_{s_\gamma\sigma_\gamma}\psi_{s_\delta\sigma_\delta}\psi_{s_\beta\sigma_\beta}\bar{s}^\mu_{s_\alpha s_\beta}\bar{s}^\mu_{s_\gamma s_\delta}\bar{\sigma}^\nu_{\sigma_\alpha\sigma_\beta}\bar{\sigma}^\nu_{\sigma_\gamma\sigma_\delta}.\end{aligned} \tag{B9}$$

For example, if we take $\mu = x$ and $\nu = y$, the Cooper pairing channel is given as follows:

$$\begin{aligned}\mathcal{S} = \frac{V^{\mathcal{Q}}}{4}\{&-\hat{\mathcal{P}}^{00,\dagger}\hat{\mathcal{P}}^{00} + \hat{\mathcal{P}}^{0x,\dagger}\hat{\mathcal{P}}^{0x} - \hat{\mathcal{P}}^{0y,\dagger}\hat{\mathcal{P}}^{0y} + \hat{\mathcal{P}}^{0z,\dagger}\hat{\mathcal{P}}^{0z} \\ &- \hat{\mathcal{P}}^{x0,\dagger}\hat{\mathcal{P}}^{x0} + \hat{\mathcal{P}}^{xx,\dagger}\hat{\mathcal{P}}^{xx} - \hat{\mathcal{P}}^{xy,\dagger}\hat{\mathcal{P}}^{xy} + \hat{\mathcal{P}}^{xz,\dagger}\hat{\mathcal{P}}^{xz} \\ &+ \hat{\mathcal{P}}^{y0,\dagger}\hat{\mathcal{P}}^{y0} - \hat{\mathcal{P}}^{yx,\dagger}\hat{\mathcal{P}}^{yx} + \hat{\mathcal{P}}^{yy,\dagger}\hat{\mathcal{P}}^{yy} - \hat{\mathcal{P}}^{yz,\dagger}\hat{\mathcal{P}}^{yz} \\ &+ \hat{\mathcal{P}}^{z0,\dagger}\hat{\mathcal{P}}^{z0} - \hat{\mathcal{P}}^{zx,\dagger}\hat{\mathcal{P}}^{zx} + \hat{\mathcal{P}}^{zy,\dagger}\hat{\mathcal{P}}^{zy} - \hat{\mathcal{P}}^{zz,\dagger}\hat{\mathcal{P}}^{zz}\}.\end{aligned} \tag{B10}$$

APPENDIX C: BARE MULTIPOLE SUSCEPTIBILITY

When we ignore the self-energy, the bare multipole susceptibility $\chi^{0,\mathcal{Q}}(q)$ can be expressed in the band basis as

$$\begin{aligned}\chi^{0,\mathcal{Q}}(q) &= \bar{\mathcal{Q}}_{\beta\alpha}\chi^{(0)}_{\alpha\beta\gamma\delta}(q)\bar{\mathcal{Q}}_{\gamma\delta} \\ &= -\bar{\mathcal{Q}}_{\beta\alpha}\frac{T}{N}\sum_k G_{\alpha\gamma}(k)G_{\delta\beta}(k-q)\bar{\mathcal{Q}}_{\gamma\delta} \\ &= -\bar{\mathcal{Q}}_{\beta\alpha}\frac{T}{N}\sum_k U_{\alpha\zeta}(\boldsymbol{k})\mathcal{G}_\zeta(k)U^*_{\gamma\zeta}(\boldsymbol{k}) \\ &\quad\times U_{\delta\eta}(\boldsymbol{k}-\boldsymbol{q})\mathcal{G}_\eta(k-q)U^*_{\beta\eta}(\boldsymbol{k}-\boldsymbol{q})\bar{\mathcal{Q}}_{\gamma\delta} \\ &= \sum_{\boldsymbol{k}}[U^\dagger(\boldsymbol{k}-\boldsymbol{q})\bar{\mathcal{Q}}U(\boldsymbol{k})]_{\eta\zeta} \\ &\quad\times[U^\dagger(\boldsymbol{k})\bar{\mathcal{Q}}U(\boldsymbol{k}-\boldsymbol{q})]_{\zeta\eta} \\ &\quad\times -\frac{T}{N}\sum_{i\omega_n}\mathcal{G}_\zeta(k)\mathcal{G}_\eta(k-q) \\ &= \sum_{\boldsymbol{k}}\mathcal{Q}^{\boldsymbol{k}-\boldsymbol{q},\boldsymbol{k}}_{\eta\zeta}\mathcal{Q}^{\boldsymbol{k},\boldsymbol{k}-\boldsymbol{q}}_{\zeta\eta}L_{\zeta\eta}(\boldsymbol{k},\boldsymbol{q},i\nu_n).\end{aligned} \tag{C1}$$

Here, $U(\boldsymbol{k})_{\alpha\zeta} = \langle\alpha|u_{\zeta,\boldsymbol{k}}\rangle$ represents the unitary matrix that diagonalizes the Hamiltonian,

$$U^\dagger(\boldsymbol{k})\mathcal{H}(\boldsymbol{k})U(\boldsymbol{k}) = \mathcal{H}^{\mathrm{diag}}(\boldsymbol{k}), \tag{C2}$$

$$\mathcal{H}(\boldsymbol{k})\,|u_{\zeta,\boldsymbol{k}}\rangle = \varepsilon_\zeta(\boldsymbol{k})\,|u_{\zeta,\boldsymbol{k}}\rangle\,. \tag{C3}$$

The Green function in the band basis is given by

$$\begin{aligned}\mathcal{G}(k) &= U^\dagger(\boldsymbol{k})G(k)U(\boldsymbol{k}), \\ \mathcal{G}_\zeta(k) &= \frac{1}{i\omega_n - \varepsilon_\zeta(\boldsymbol{k})}.\end{aligned} \tag{C4}$$

APPENDIX D: MULTIPOLE-RESOLVED EFFECTIVE INTERACTION

Similar to Eq. (12), we can decompose the effective interaction $\Gamma^n(q)$ [as defined in Eq. (A4)] and $\Gamma^a(q)$ [as defined in Eq. (A11)] into their respective multipole channels. The decomposition is expressed as follows:

$$\Gamma^{n,\mathcal{Q}}(q) \approx U^{\mathcal{Q}}\left[\chi^{\mathcal{Q}}(q) - \tfrac{1}{2}\chi^{0,\mathcal{Q}}(q)\right]U^{\mathcal{Q}}, \tag{D1}$$

$$\Gamma^{a,\mathcal{Q}}(q) \approx \frac{U^{\mathcal{Q}}}{2} + U^{\mathcal{Q}}\chi^{\mathcal{Q}}(q)U^{\mathcal{Q}}. \tag{D2}$$

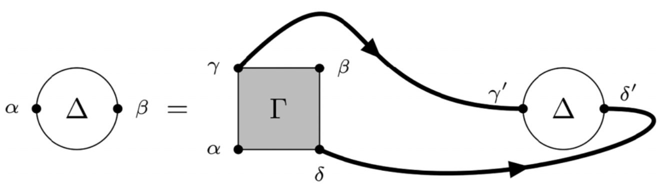

FIG. 5. The diagrammatic representation of the Éliashberg equation. The shaded square and the black line represent the irreducible four-point vertex function in the particle-particle channel and the single-particle Green function, respectively.

In Eq. (D1), the effective interaction for the particle-hole channel, $\Gamma^{n,\mathcal{Q}}(q)$, is expressed as a function of the multipole susceptibility $\chi^{\mathcal{Q}}(q)$ and the bare susceptibility $\chi^{0,\mathcal{Q}}(q)$ modulated by the interaction $U^{\mathcal{Q}}$. Similarly, Eq. (D2) depicts the effective interaction for the particle-particle channel, $\Gamma^{a,\mathcal{Q}}(q)$, also as a function of the multipole susceptibility and interaction.

APPENDIX E: ÉLIASHBERG EQUATION

To investigate superconductivity, we adopt the linearized Éliashberg equation, which is expressed as

$$\lambda\Delta_{\alpha\beta}(k) = \frac{T}{N}\sum_{k'}\Gamma^{a}_{\alpha\gamma\delta\beta}(k-k')G_{\gamma\gamma'}(k)\Delta_{\gamma'\delta'}(k)G_{\delta\delta'}(-k), \tag{E1}$$

where Δ is the gap function and Γ^{a} is the particle-particle channel irreducible vertex function obtained in Eq. (A11). Figure 5 shows the diagrammatic representation of the linearized Éliashberg equation. With the power method, we numerically evaluate λ, eigenvalues of the linearized Éliashberg equation, and determine the critical temperature T_c from the criterion $\lambda = 1$.

[1] M. Tinkham, *Introduction to Superconductivity*, 2nd ed. (Dover, Mineola, NY, 2004).
[2] V. Jaccarino and M. Peter, Ultra-high-field superconductivity, Phys. Rev. Lett. **9**, 290 (1962).
[3] O. H. Fischer, Properties of high-field superconductors containing localized magnetic moments, Helv. Phys. Acta. **45**, 331 (1972).
[4] H. W. Meul, C. Rossel, M. Decroux, O. Fischer, G. Remenyi, and A. Briggs, Observation of magnetic-field-induced superconductivity, Phys. Rev. Lett. **53**, 497 (1984).
[5] O. Fischer, H. W. Meul, M. G. Karkut, G. Remenyi, U. Welp, J. C. Piccoche, and K. Maki, Antivortex paramagnetism in the magnetic-field-induced superconducting state of $Eu_xSn_{1-x}Mo_6S_8$, Phys. Rev. Lett. **55**, 2972 (1985).
[6] S. Uji, H. Shinagawa, T. Terashima, T. Yakabe, Y. Terai, M. Tokumoto, A. Kobayashi, H. Tanaka, and H. Kobayashi, Magnetic-field-induced superconductivity in a two-dimensional organic conductor, Nature (London) **410**, 908 (2001).
[7] L. Balicas, J. S. Brooks, K. Storr, S. Uji, M. Tokumoto, H. Tanaka, H. Kobayashi, A. Kobayashi, V. Barzykin, and L. P. Gor'kov, Superconductivity in an organic insulator at very high magnetic fields, Phys. Rev. Lett. **87**, 067002 (2001).
[8] T. Konoike, S. Uji, T. Terashima, M. Nishimura, S. Yasuzuka, K. Enomoto, H. Fujiwara, B. Zhang, and H. Kobayashi, Magnetic-field-induced superconductivity in the antiferromagnetic organic superconductor κ-$(BETS)_2FeBr_4$, Phys. Rev. B **70**, 094514 (2004).
[9] A. N. Podmarkov and I. S. Sandalov, Recovery of superconductivity suppressed by magnetic impurities by use of a magnetic field, Supercond. Sci. Technol. **2**, 66 (1989).
[10] A. N. Podmarkov and I. S. Sandalov, Possibility of magnetic-field-induced superconductivity in a metal with Kondo impurities, Zh. Eksp. Teor. Fiz. **95**, 2235 (1989) [J. Expt. Theor. Phys. **68**, 1291 (1989)].
[11] M. Tachiki, B. D. Dunlap, G. W. Crabtree, S. Takahashi, and T. Koyama, Unusual temperature dependence of the upper critical field in superconducting heavy-fermion systems, Phys. Rev. B **34**, 7603 (1986).
[12] S. S. Saxena, P. Agarwal, K. Ahilan, F. M. Grosche, R. K. W. Haselwimmer, M. J. Steiner, E. Pugh, I. R. Walker, S. R. Julian, P. Monthoux, G. G. Lonzarich, A. Huxley, I. Sheikin, D. Braithwaite, and J. Flouquet, Superconductivity on the border of itinerant-electron ferromagnetism in UGe_2, Nature (London) **406**, 587 (2000).
[13] I. Sheikin, A. Huxley, D. Braithwaite, J. P. Brison, S. Watanabe, K. Miyake, and J. Flouquet, Anisotropy and pressure dependence of the upper critical field of the ferromagnetic superconductor UGe_2, Phys. Rev. B **64**, 220503(R) (2001).
[14] D. Aoki, A. Huxley, E. Ressouche, D. Braithwaite, J. Flouquet, J.-P. Brison, E. Lhotel, and C. Paulsen, Coexistence of superconductivity and ferromagnetism in URhGe, Nature (London) **413**, 613 (2001).
[15] F. Lévy, I. Sheikin, B. Grenier, and A. D. Huxley, Magnetic field-induced superconductivity in the ferromagnet URhGe, Science **309**, 1343 (2005).
[16] N. T. Huy, A. Gasparini, D. E. de Nijs, Y. Huang, J. C. P. Klaasse, T. Gortenmulder, A. de Visser, A. Hamann, T. Görlach, and H. v. Löhneysen, Superconductivity on the border of weak itinerant ferromagnetism in UCoGe, Phys. Rev. Lett. **99**, 067006 (2007).
[17] D. Aoki, T. D. Matsuda, V. Taufour, E. Hassinger, G. Knebel, and J. Flouquet, Extremely large and anisotropic upper critical field and the ferromagnetic instability in UCoGe, J. Phys. Soc. Jpn. **78**, 113709 (2009).
[18] S. Ran, C. Eckberg, Q.-P. Ding, Y. Furukawa, T. Metz, S. R. Saha, I.-L. Liu, M. Zic, H. Kim, J. Paglione, and N. P. Butch, Nearly ferromagnetic spin-triplet superconductivity, Science **365**, 684 (2019).
[19] D. Aoki, A. Nakamura, F. Honda, D. Li, Y. Homma, Y. Shimizu, Y. J. Sato, G. Knebel, J.-P. Brison, A. Pourret, D. Braithwaite, G. Lapertot, Q. Niu, M. Vališka, H. Harima, and J. Flouquet, Unconventional superconductivity in heavy fermion UTe_2, J. Phys. Soc. Jpn. **88**, 043702 (2019).

[20] S. Ran, I.-L. Liu, Y. S. Eo, D. J. Campbell, P. M. Neves, W. T. Fuhrman, S. R. Saha, C. Eckberg, H. Kim, D. Graf, F. Balakirev, J. Singleton, J. Paglione, and N. P. Butch, Extreme magnetic field-boosted superconductivity, Nat. Phys. **15**, 1250 (2019).

[21] G. Knebel, W. Knafo, A. Pourret, Q. Niu, M. Vališka, D. Braithwaite, G. Lapertot, M. Nardone, A. Zitouni, S. Mishra, I. Sheikin, G. Seyfarth, J.-P. Brison, D. Aoki, and J. Flouquet, Field-Reentrant superconductivity close to a metamagnetic transition in the heavy-fermion superconductor UTe_2, J. Phys. Soc. Jpn. **88**, 063707 (2019).

[22] T. Hattori, Y. Ihara, Y. Nakai, K. Ishida, Y. Tada, S. Fujimoto, N. Kawakami, E. Osaki, K. Deguchi, N. K. Sato, and I. Satoh, Superconductivity induced by longitudinal ferromagnetic fluctuations in UCoGe, Phys. Rev. Lett. **108**, 066403 (2012).

[23] K. Hattori and H. Tsunetsugu, p-wave superconductivity near a transverse saturation field, Phys. Rev. B **87**, 064501 (2013).

[24] Y. Tada, S. Fujimoto, N. Kawakami, T. Hattori, Y. Ihara, K. Ishida, K. Deguchi, N. K. Sato, and I. Satoh, Spin-Triplet superconductivity induced by longitudinal ferromagnetic fluctuations in UCoGe: Theoretical aspect, J. Phys.: Conf. Ser. **449**, 012029 (2013).

[25] T. Hattori, K. Karube, K. Ishida, K. Deguchi, N. K. Sato, and T. Yamamura, Relationship between ferromagnetic criticality and the enhancement of superconductivity induced by transverse magnetic fields in UCoGe, J. Phys. Soc. Jpn. **83**, 073708 (2014).

[26] Y. Tokunaga, D. Aoki, H. Mayaffre, S. Krämer, M.-H. Julien, C. Berthier, M. Horvatić, H. Sakai, S. Kambe, and S. Araki, Reentrant superconductivity driven by quantum tricritical fluctuations in URhGe: Evidence from ^{59}Co NMR in $URh_{0.9}Co_{0.1}Ge$, Phys. Rev. Lett. **114**, 216401 (2015).

[27] Y. Tokunaga, D. Aoki, H. Mayaffre, S. Krämer, M.-H. Julien, C. Berthier, M. Horvatić, H. Sakai, T. Hattori, S. Kambe, and S. Araki, Interplay between quantum fluctuations and reentrant superconductivity with a highly enhanced upper critical field in URhGe, Phys. Rev. B **93**, 201112(R) (2016).

[28] Y. Tada, S. Takayoshi, and S. Fujimoto, Magnetism and superconductivity in ferromagnetic heavy-fermion system UCoGe under in-plane magnetic fields, Phys. Rev. B **93**, 174512 (2016).

[29] B. Wu, G. Bastien, M. Taupin, C. Paulsen, L. Howald, D. Aoki, and J.-P. Brison, Pairing mechanism in the ferromagnetic superconductor UCoGe, Nat. Commun. **8**, 14480 (2017).

[30] A. Rosuel, C. Marcenat, G. Knebel, T. Klein, A. Pourret, N. Marquardt, Q. Niu, S. Rousseau, A. Demuer, G. Seyfarth, G. Lapertot, D. Aoki, D. Braithwaite, J. Flouquet, and J. P. Brison, Field-induced tuning of the pairing state in a superconductor, Phys. Rev. X **13**, 011022 (2023).

[31] S. Khim, J. F. Landaeta, J. Banda, N. Bannor, M. Brando, P. M. R. Brydon, D. Hafner, R. Küchler, R. Cardoso-Gil, U. Stockert, A. P. Mackenzie, D. F. Agterberg, C. Geibel, and E. Hassinger, Field-induced transition within the superconducting state of $CeRh_2As_2$, Science **373**, 1012 (2021).

[32] E. G. Schertenleib, M. H. Fischer, and M. Sigrist, Unusual H-T phase diagram of $CeRh_2As_2$: The role of staggered noncentrosymmetricity, Phys. Rev. Res. **3**, 023179 (2021).

[33] D. Möckli and A. Ramires, Two scenarios for superconductivity in $CeRh_2As_2$, Phys. Rev. Res. **3**, 023204 (2021).

[34] A. Ptok, K. J. Kapcia, P. T. Jochym, J. Łażewski, A. M. Oleś, and P. Piekarz, Electronic and dynamical properties of $CeRh_2As_2$: Role of Rh_2As_2 layers and expected orbital order, Phys. Rev. B **104**, L041109 (2021).

[35] K. Nogaki, A. Daido, J. Ishizuka, and Y. Yanase, Topological crystalline superconductivity in locally noncentrosymmetric $CeRh_2As_2$, Phys. Rev. Res. **3**, L032071 (2021).

[36] D. Möckli and A. Ramires, Superconductivity in disordered locally noncentrosymmetric materials: An application to $CeRh_2As_2$, Phys. Rev. B **104**, 134517 (2021).

[37] S. I. Kimura, J. Sichelschmidt, and S. Khim, Optical study of the electronic structure of locally noncentrosymmetric $CeRh_2As_2$, Phys. Rev. B **104**, 245116 (2021).

[38] S. Onishi, U. Stockert, S. Khim, J. Banda, M. Brando, and E. Hassinger, Low-Temperature thermal conductivity of the two-phase superconductor $CeRh_2As_2$, Front. Electron. Mater. **2**, 880579 (2022).

[39] D. C. Cavanagh, T. Shishidou, M. Weinert, P. M. R. Brydon, and D. F. Agterberg, Nonsymmorphic symmetry and field-driven odd-parity pairing in $CeRh_2As_2$, Phys. Rev. B **105**, L020505 (2022).

[40] D. Hafner, P. Khanenko, E.-O. Eljaouhari, R. Küchler, J. Banda, N. Bannor, T. Lühmann, J. F. Landaeta, S. Mishra, I. Sheikin, E. Hassinger, S. Khim, C. Geibel, G. Zwicknagl, and M. Brando, Possible quadrupole density wave in the superconducting Kondo lattice $CeRh_2As_2$, Phys. Rev. X **12**, 011023 (2022).

[41] M. Kibune, S. Kitagawa, K. Kinjo, S. Ogata, M. Manago, T. Taniguchi, K. Ishida, M. Brando, E. Hassinger, H. Rosner, C. Geibel, and S. Khim, Observation of antiferromagnetic order as odd-parity multipoles inside the superconducting phase in $CeRh_2As_2$, Phys. Rev. Lett. **128**, 057002 (2022).

[42] S. Kitagawa, M. Kibune, K. Kinjo, M. Manago, T. Taniguchi, K. Ishida, M. Brando, E. Hassinger, C. Geibel, and S. Khim, Two-Dimensional XY-Type magnetic properties of locally noncentrosymmetric superconductor $CeRh_2As_2$, J. Phys. Soc. Jpn. **91**, 043702 (2022).

[43] T. Hazra and P. Coleman, Triplet pairing mechanisms from Hund's-Kondo models: Applications to UTe_2 and $CeRh_2As_2$, Phys. Rev. Lett. **130**, 136002 (2023).

[44] K. Nogaki and Y. Yanase, Even-odd parity transition in strongly correlated locally noncentrosymmetric superconductors: Application to $CeRh_2As_2$, Phys. Rev. B **106**, L100504 (2022).

[45] J. F. Landaeta, P. Khanenko, D. C. Cavanagh, C. Geibel, S. Khim, S. Mishra, I. Sheikin, P. M. R. Brydon, D. F. Agterberg, M. Brando, and E. Hassinger, Field-Angle dependence reveals odd-parity superconductivity in $CeRh_2As_2$, Phys. Rev. X **12**, 031001 (2022).

[46] K. Machida, Violation of Pauli-Clogston limit in the heavy-fermion superconductor $CeRh_2As_2$: Duality of itinerant and localized $4f$ electrons, Phys. Rev. B **106**, 184509 (2022).

[47] H. Siddiquee, Z. Rehfuss, C. Broyles, and S. Ran, Pressure dependence of superconductivity in $CeRh_2As_2$, Phys. Rev. B **108**, L020504 (2023).

[48] S. Mishra, Y. Liu, E. D. Bauer, F. Ronning, and S. M. Thomas, Anisotropic magnetotransport properties of the heavy-fermion superconductor $CeRh_2As_2$, Phys. Rev. B **106**, L140502 (2022).

[49] C. Lee and S. B. Chung, Linear optical response from the odd-parity Bardasis-Schrieffer mode in locally noncentrosymmetric superconductors, Commun. Phys. **6**, 307 (2023).

[50] K. Semeniuk, D. Hafner, P. Khanenko, T. Lühmann, J. Banda, J. F. Landaeta, C. Geibel, S. Khim, E. Hassinger, and M. Brando, Decoupling multiphase superconductivity from normal state ordering in $CeRh_2As_2$, Phys. Rev. B **107**, L220504 (2023).

[51] S. Ogata, S. Kitagawa, K. Kinjo, K. Ishida, M. Brando, E. Hassinger, C. Geibel, and S. Khim, Parity transition of spin-singlet superconductivity using sublattice degrees of freedom, Phys. Rev. Lett. **130**, 166001 (2023).

[52] N. A. Hackner and P. M. R. Brydon, Bardasis-Schrieffer-like phase mode in a superconducting bilayer, Phys. Rev. B **108**, L220505 (2023).

[53] A. L. Szabó, M. H. Fischer, and M. Sigrist, Effects of nucleation at a first-order transition between two superconducting phases: Application to $cerh_2as_2$, Phys. Rev. Res. **6**, 023080 (2024).

[54] D. S. Christovam, M. Ferreira-Carvalho, A. Marino, M. Sundermann, D. Takegami, A. Melendez-Sans, K. D. Tsuei, Z. Hu, S. Rößler, M. Valvidares, M. W. Haverkort, Y. Liu, E. D. Bauer, L. H. Tjeng, G. Zwicknagl, and A. Severing, Spectroscopic evidence of Kondo-induced quasiquartet in $CeRh_2As_2$, Phys. Rev. Lett. **132**, 046401 (2024).

[55] A. Szabo and A. Ramires, Superconductivity-induced improper orders, arXiv:2309.05664.

[56] X. Chen, L. Wang, J. Ishizuka, R. Zhang, K. Nogaki, Y. Cheng, F. Yang, Z. Chen, F. Zhu, Z. Liu, J. Mei, Y. Yanase, B. Lv, and Y. Huang, Coexistence of near-E_F flat band and van hove singularity in a two-phase superconductor, Phys. Rev. X **14**, 021048 (2024).

[57] Y. Wu, Y. Zhang, S. Ju, Y. Hu, Y. Huang, Y. Zhang, H. Zhang, H. Zheng, G. Yang, E.-O. Eljaouhari, B. Song, N. C. Plumb, F. Steglich, M. Shi, G. Zwicknagl, C. Cao, H. Yuan, and Y. Liu, Fermi surface nesting with heavy quasiparticles in the locally noncentrosymmetric superconductor $CeRh_2As_2$, Chin. Phys. Lett. **41**, 097403 (2024).

[58] J. Ishizuka, K. Nogaki, M. Sigrist, and Y. Yanase, Correlation-induced Fermi surface evolution and topological crystalline superconductivity in $CeRh_2As_2$, Phys. Rev. B **110**, L140505 (2024).

[59] P. C. Canfield, J. D. Thompson, and Z. Fisk, Novel Ce magnetism in CeDipnictide and Di-Ce pnictide structures, J. Appl. Phys. **70**, 5992 (1991).

[60] O. P. Squire, S. A. Hodgson, J. Chen, V. Fedoseev, C. K. de Podesta, T. I. Weinberger, P. L. Alireza, and F. M. Grosche, Superconductivity beyond the conventional Pauli limit in high-pressure $CeSb_2$, Phys. Rev. Lett. **131**, 026001 (2023).

[61] J. M. Park, Y. Cao, K. Watanabe, T. Taniguchi, and P. Jarillo-Herrero, Tunable strongly coupled superconductivity in magic-angle twisted trilayer graphene, Nature (London) **590**, 249 (2021).

[62] Y. Cao, J. M. Park, K. Watanabe, T. Taniguchi, and P. Jarillo-Herrero, Pauli-limit violation and re-entrant superconductivity in Moiré graphene, Nature (London) **595**, 526 (2021).

[63] H. Watanabe and Y. Yanase, Group-theoretical classification of multipole order: Emergent responses and candidate materials, Phys. Rev. B **98**, 245129 (2018).

[64] S. Hayami, M. Yatsushiro, Y. Yanagi, and H. Kusunose, Classification of atomic-scale multipoles under crystallographic point groups and application to linear response tensors, Phys. Rev. B **98**, 165110 (2018).

[65] M. Yatsushiro, H. Kusunose, and S. Hayami, Multipole classification in 122 magnetic point groups for unified understanding of multiferroic responses and transport phenomena, Phys. Rev. B **104**, 054412 (2021).

[66] V. Kozii and L. Fu, Odd-parity superconductivity in the vicinity of inversion symmetry breaking in spin-orbit-coupled systems, Phys. Rev. Lett. **115**, 207002 (2015).

[67] T. Nomoto, K. Hattori, and H. Ikeda, Classification of "multipole" superconductivity in multiorbital systems and its implications, Phys. Rev. B **94**, 174513 (2016).

[68] S. Sumita and Y. Yanase, Superconductivity in magnetic multipole states, Phys. Rev. B **93**, 224507 (2016).

[69] S. Sumita, T. Nomoto, and Y. Yanase, Multipole superconductivity in nonsymmorphic Sr_2IrO_4, Phys. Rev. Lett. **119**, 027001 (2017).

[70] J. Ishizuka and Y. Yanase, Odd-parity multipole fluctuation and unconventional superconductivity in locally noncentrosymmetric crystal, Phys. Rev. B **98**, 224510 (2018).

[71] S. Sumita and Y. Yanase, Superconductivity induced by fluctuations of momentum-based multipoles, Phys. Rev. Res. **2**, 033225 (2020).

[72] J. C. Ward, An identity in quantum electrodynamics, Phys. Rev. **78**, 182 (1950).

[73] Y. Takahashi, On the generalized ward identity, Nuovo Cim. **6**, 371 (1957).

[74] N. E. Bickers, D. J. Scalapino, and S. R. White, Conserving approximations for strongly correlated electron Systems: Bethe-Salpeter equation and dynamics for the two-dimensional hubbard model, Phys. Rev. Lett. **62**, 961 (1989).

[75] N. Bickers and D. Scalapino, Conserving approximations for strongly fluctuating electron systems. I. Formalism and calculational approach, Ann. Phys. **193**, 206 (1989).

[76] N. E. Bickers and S. R. White, Conserving approximations for strongly fluctuating electron systems. II. Numerical results and parquet extension, Phys. Rev. B **43**, 8044 (1991).

[77] B. Roulet, J. Gavoret, and P. Nozières, Singularities in the x-ray absorption and emission of metals. I. First-order parquet calculation, Phys. Rev. **178**, 1072 (1969).

[78] N. E. Bickers, Self-Consistent many-body theory for condensed matter systems, in *Theoretical Methods for Strongly Correlated Electrons*, edited by D. Sénéchal, A.-M. Tremblay, and C. Bourbonnais (Springer, New York, 2004), pp. 237–296.

[79] Y. Yanase, Random spin-orbit coupling in spin triplet superconductors: Stacking faults in Sr_2RuO_4 and $CePt_3Si$, J. Phys. Soc. Jpn. **79**, 084701 (2010).

[80] M. H. Fischer, F. Loder, and M. Sigrist, Superconductivity and local noncentrosymmetricity in crystal lattices, Phys. Rev. B **84**, 184533 (2011).

[81] D. Maruyama, M. Sigrist, and Y. Yanase, Locally noncentrosymmetric superconductivity in multilayer systems, J. Phys. Soc. Jpn. **81**, 034702 (2012).

[82] T. Yoshida, M. Sigrist, and Y. Yanase, Pair-density wave states through spin-orbit coupling in multilayer superconductors, Phys. Rev. B **86**, 134514 (2012).

[83] D. Maruyama, M. Sigrist, and Y. Yanase, Spin–orbit coupling in multilayer superconductors with charge imbalance, J. Phys. Soc. Jpn. **82**, 043703 (2013).

[84] T. Yoshida, M. Sigrist, and Y. Yanase, Complex-Stripe phases induced by staggered Rashba spin–orbit coupling, J. Phys. Soc. Jpn. **82**, 074714 (2013).

[85] T. Yoshida, M. Sigrist, and Y. Yanase, Parity-Mixed superconductivity in locally non-centrosymmetric system, J. Phys. Soc. Jpn. **83**, 013703 (2014).

[86] T. Yoshida, M. Sigrist, and Y. Yanase, Topological crystalline superconductivity in locally noncentrosymmetric multilayer superconductors, Phys. Rev. Lett. **115**, 027001 (2015).

[87] T. Hitomi and Y. Yanase, Electric octupole order in bilayer Rashba system, J. Phys. Soc. Jpn. **85**, 124702 (2016).

[88] D. Möckli, Y. Yanase, and M. Sigrist, Orbitally limited pair-density-wave phase of multilayer superconductors, Phys. Rev. B **97**, 144508 (2018).

[89] X. Lu and D. Sénéchal, Spin texture in a bilayer high-temperature cuprate superconductor, Phys. Rev. B **104**, 024502 (2021).

[90] A. Skurativska, M. Sigrist, and M. H. Fischer, Spin response and topology of a staggered-Rashba superconductor, Phys. Rev. Res. **3**, 033133 (2021).

[91] E. Bauer and M. Sigrist, *Noncentrosymmetric Superconductors: Introduction and Overview* (Springer Science & Business Media, New York, 2012), Vol. 847.

[92] It should be noted that extending the current discussion to cases with general N degrees of freedom is straightforward. This involves replacing the Pauli matrix with the $\mathfrak{su}(N)$ Lie algebra.

[93] Edited by S. Sugano, Y. Tanabe, and H. Kamimura, Two electrons in a cubic field, in *Multiplets of Transition-Metal Ions in Crystals*, Pure and Applied Physics, Vol. 33 (Elsevier, Amsterdam, 1970), pp. 38–65.

[94] A. C. Simmonett, I. Pickard, C. Frank, I. Schaefer, F. Henry, and B. R. Brooks, An efficient algorithm for multipole energies and derivatives based on spherical harmonics and extensions to particle mesh Ewald, J. Chem. Phys. **140**, 184101 (2014).

[95] M. E. A. Coury, S. L. Dudarev, W. M. C. Foulkes, A. P. Horsfield, P.-W. Ma, and J. S. Spencer, Hubbard-like Hamiltonians for interacting electrons in s, p, and d orbitals, Phys. Rev. B **93**, 075101 (2016).

[96] J. Bünemann and F. Gebhard, Coulomb matrix elements in multi-orbital Hubbard models, J. Phys.: Condens. Matter **29**, 165601 (2017).

[97] S. Iimura, M. Hirayama, and S. Hoshino, Multipole representation for anisotropic Coulomb interactions, Phys. Rev. B **104**, L081108 (2021).

[98] S. J. Youn, M. H. Fischer, S. H. Rhim, M. Sigrist, and D. F. Agterberg, Role of strong spin-orbit coupling in the superconductivity of the hexagonal pnictide SrPtAs, Phys. Rev. B **85**, 220505(R) (2012).

[99] J. Goryo, M. H. Fischer, and M. Sigrist, Possible pairing symmetries in SrPtAs with a local lack of inversion center, Phys. Rev. B **86**, 100507(R) (2012).

[100] J. M. Luttinger and J. C. Ward, Ground-State energy of a many-fermion system. II, Phys. Rev. **118**, 1417 (1960).

[101] J. M. Luttinger, Fermi surface and some simple equilibrium properties of a system of interacting fermions, Phys. Rev. **119**, 1153 (1960).

[102] G. Baym and L. P. Kadanoff, Conservation laws and correlation functions, Phys. Rev. **124**, 287 (1961).

[103] G. Baym, Self-consistent approximations in many-body systems, Phys. Rev. **127**, 1391 (1962).

[104] H. Yao and F. Yang, Topological odd-parity superconductivity at type-II two-dimensional van Hove singularities, Phys. Rev. B **92**, 035132 (2015).

[105] X. Wu, M. Fink, W. Hanke, R. Thomale, and D. Di Sante, Unconventional superconductivity in a doped quantum spin Hall insulator, Phys. Rev. B **100**, 041117(R) (2019).

[106] K. Nogaki and Y. Yanase, Strongly parity-mixed superconductivity in the Rashba-Hubbard model, Phys. Rev. B **102**, 165114 (2020).

[107] T. Moriya and K. Ueda, Spin fluctuations and high temperature superconductivity, Adv. Phys. **49**, 555 (2000).

[108] Y. Yanase, T. Jujo, T. Nomura, H. Ikeda, T. Hotta, and K. Yamada, Theory of superconductivity in strongly correlated electron systems, Phys. Rep. **387**, 1 (2003).

[109] M. Houzet and A. Buzdin, Nonuniform superconducting phases in a layered ferromagnetic superconductor, Europhys. Lett. **58**, 596 (2002).

[110] A. Buzdin, S. Tollis, and J. Cayssol, Field-induced superconductivity with an enhanced and tunable paramagnetic limit, Phys. Rev. Lett. **95**, 167003 (2005).

[111] S. Tollis, J. Cayssol, and A. Buzdin, Competition between π-coupling and Fulde-Ferrell-Larkin-Ovchinnikov modulation in a periodic array of ferromagnetic-superconducting bilayers of atomic thickness, Phys. Rev. B **73**, 174519 (2006).

[112] A. Buzdin, S. Tollis, and J. Cayssol, Anomalous (H,T) phase diagram in bilayered superconducting systems, Physica C: Superconductivity **460-462**, 1028 (2007).

[113] X. Montiel and A. I. Buzdin, Field-induced superconducting phase in superconductor–normal metal and superconductor-superconductor bilayers, Phys. Rev. B **84**, 054518 (2011).

[114] E. Khalaf, A. J. Kruchkov, G. Tarnopolsky, and A. Vishwanath, Magic angle hierarchy in twisted graphene multilayers, Phys. Rev. B **100**, 085109 (2019).

[115] S. Carr, C. Li, Z. Zhu, E. Kaxiras, S. Sachdev, and A. Kruchkov, Ultraheavy and ultrarelativistic Dirac quasiparticles in sandwiched graphenes, Nano Lett. **20**, 3030 (2020).

[116] C. Lei, L. Linhart, W. Qin, F. Libisch, and A. H. MacDonald, Mirror symmetry breaking and lateral stacking shifts in twisted trilayer graphene, Phys. Rev. B **104**, 035139 (2021).

[117] S. Onari and H. Kontani, SU(4) Valley + Spin Fluctuation interference mechanism for nematic order in magic-angle twisted bilayer graphene: The impact of vertex corrections, Phys. Rev. Lett. **128**, 066401 (2022).

[118] M. Kawamura, FermiSurfer: Fermi-surface viewer providing multiple representation schemes, Comput. Phys. Commun. **239**, 197 (2019).